The Relative Warming Rates of Heat Events and Median Days in the Pacific Northwest from Observations and a Regional Climate Model

Eric P Salathé Jr[a], Adrienne Beggs[a,b], Chris McJunkin[a], and Satveer Sandhu[a]

[a] *University of Washington Bothell, Bothell, Washington*

[b] *Berea College, Berea KY*

Corresponding author: Eric Salathé, salathe@uw.edu

Early Online Release: This preliminary version has been accepted for publication in *Journal of Climate*, may be fully cited, and has been assigned DOI 10.1175/JCLI-D-22-0313.1. The final typeset copyedited article will replace the EOR at the above DOI when it is published.

Abstract

This paper examines the trends in hot summer days for the Pacific Northwest in observations and a regional climate model ensemble. Hot days are identified by the temperature threshold for several percentile values computed over 10-year intervals (85, 90, 95, and absolute maximum) to differentiate heat events of different intensities and are compared to the median temperature (50th percentile). For the stations analyzed, the observed rate of warming during hot days is not statistically different from the warming rate of median days since the 1950s. However, for projections to 2100, hot days show a statistically significant increase in the warming rate of the hottest days compared to the warming rate for median days. Depending on location, the 95th percentile daily maximum temperature shows a warming rate of up to 0.2°C per decade above the median warming rate. The divergence in the trends of median and extreme temperature shows substantial regional variation depending on local terrain and coastlines. The warming trend during hot days is related to the unique circulation patterns during heat events, which respond to different feedbacks and amplifying effects in the land-atmosphere system from those that prevail during typical days. The regional climate model simulations are taken from an ensemble of Weather Research and Forecasting (WRF) model simulations forced by 12 global climate model simulations from the 5th Climate Model Intercomparison Project (CMIP5) using the RCP8.5 emissions scenario and 12-km grid spacing.

Significance Statement

The heat wave of June 2021 had substantial societal and ecological impacts, illustrating vulnerability to record shattering events. This paper addresses whether climate change can cause heat events in the Pacific Northwest to warm at a more rapid rate than typical days. Based on observations, in the recent past, the hottest days warmed at about the same rate as typical days in the recent past. However, results from a high-resolution climate model show a higher rate of warming during the warmest days relative to median days under the most aggressive future emissions scenario. This effect could cause heat waves to become more intense relative to typical days by 2100, making adaptation to extreme events more difficult.

Accepted for publication in *Journal of Climate*. DOI 10.1175/JCLI-D-22-0313.1

I. Introduction

In June 2021, a severe heat event in the United States Pacific Northwest resulted in daytime high temperatures on 28 June 2021 of 42°C (108°F) at the Seattle-Tacoma (Sea-Tac), WA, and 47°C (116°F) at the Portland, OR, airport weather stations. This event exceeded the previous record high temperature at Sea-Tac by 2.8°C and at Portland by 5°C. The meteorological conditions during the event consisted of an anomalously strong and persistent high-pressure ridge over the western U.S. that yielded a combination of strong large-scale subsidence warming and anomalous easterly flow, advecting hot continental air toward the coast (Overland 2021). This rare and intense circulation pattern, within the background of steadily increasing mean temperatures, resulted in the record high temperatures. Record-shattering events like this present a significant challenge in adapting to climate change (Fischer et al. 2021). Where climate processes can cause extremes to increase more rapidly than the mean climate, the vulnerability of natural and human systems to future extreme events is substantially increased. The recent event, and its unprecedented anomaly relative to past events, clearly illustrates this concern. The region was wholly unprepared for the consequences of such temperature extremes, which resulted in a substantial increase in the human death rate, significant ecological damage, and rapid glacial collapse (Klein et al. 2022; Overland 2021). Given the adaptation challenge of rare and extreme events, it is critically important to understand how future heat events in the region respond to climate change in ways that differ from the mean climate response.

The simplest assumption is that, at least in the near term, climate change will not substantially alter the circulation patterns historically responsible for heat events. A recent study of CMIP6 climate models found the atmospheric ridge pattern during heat waves in this region is not simulated to change significantly in amplitude or frequency (Loikith et al. 2022) even under the strongest emissions scenario. In this case, one might expect the probability distribution of daily temperatures in any decade to increase uniformly with the median temperature (as for example, Fig 2.32a in Folland et al, 2001), maintaining the standard deviation and skewness of the past probability distribution so that all temperature percentiles increase at the same rate as the median. Rhines and Huybers (2013) argue this assumption is justified by the observations of summer-time average temperature and allows for most of the important features of the observed increase in extreme events due to climate change. However, Donat and Alexander (2012) found regionally-dependent shifts in the variance and skewness of daily temperature anomalies for

Accepted for publication in *Journal of Climate*. DOI 10.1175/JCLI-D-22-0313.1

1981-2010 compared to 1951-1980, and suggest that extreme events have become more extreme relative to the mean in recent decades. A number of studies hypothesize processes that could cause extreme events to change at a different rate than the mean climate, for example soil-moisture feedbacks could amplify extremes (Seneviratne et al. 2014) while weakening off-shore winds along the west coast (Brewer and Mass 2016) could reduce extremes.

Heat events in the Pacific Northwest during the warm season, which we define here as the period May through September, are typically the result of the synoptic development of a West Coast thermal trough (WCTT) (Brewer et al. 2012). The WCTT is characterized by a ridging pattern in the lower troposphere that produces offshore flow with adiabatic warming as continental air descends the west slopes of the Cascade Range. The resulting hot and dry conditions have significant impacts on the populous areas of Washington and Oregon west of the Cascades, creating heat stress, poor air quality, and increased risk of wildfire. The anomalous easterly winds and associated air parcel trajectories skew the temperature probability distribution west of the Cascades with a long warm tail (Brewer and Mass 2016; Catalano et al. 2021). The dynamics of this ridging pattern prevents the typical cooling by marine and advects air parcels from the north and east of the region (Catalano et al. 2021).

In this paper, we use historic station records of maximum daily temperature and the results of a high-resolution regional climate model ensemble to examine the relative trends in extreme and median temperatures. We seek to establish whether there has been a difference in the warming trend of extreme temperatures compared to median temperatures historically and whether a high-resolution climate model projects such a difference for the future. We focus specifically on heat waves in the Pacific Northwest, which is governed by unique meteorological and climatological conditions controlled by complex terrain and coastlines. To establish the effect of climate change on typical days and on high-temperature days, we examine the temperature within 10-year periods at multiple percentile thresholds, the median (50%), 80%, 95%, 99%, and decadal maximum of daily maximum temperature during the months May through September.

II. Regional Climate Model Ensemble

This paper analyzes an ensemble of twelve high-resolution regional climate simulations, created by dynamically downscaling CMIP5 global climate simulations (Taylor et al. 2012). This downscaling uses the National Center for Atmospheric Research (NCAR) Weather Research and

Accepted for publication in *Journal of Climate*. DOI 10.1175/JCLI-D-22-0313.1

Forecasting (WRF) model run at 12-km grid spacing, which allows realistic simulation of key mesoscale features. The simulations include a large 36-km domain with a nested 12-km domain over the northwestern U.S. The geography of the inner 12-km domain is shown in Figure 1. Ensemble results are evaluated and analyzed in detail by Mass et al (2022).

The global model simulations used in the ensemble are all based on the RCP 8.5 greenhouse gas emissions scenario, the most aggressive scenario used in CMIP5. This scenario allows simulations that explore a strong signal in the mesoscale response to climate change. However, it may well represent unrealistic greenhouse gas concentrations later in the century (Hausfather and Peters 2020), and the results presented here should not be interpreted as the most likely outcome, subject to greenhouse gas mitigation actions to avoid the extreme emissions represented in RCP 8.5.

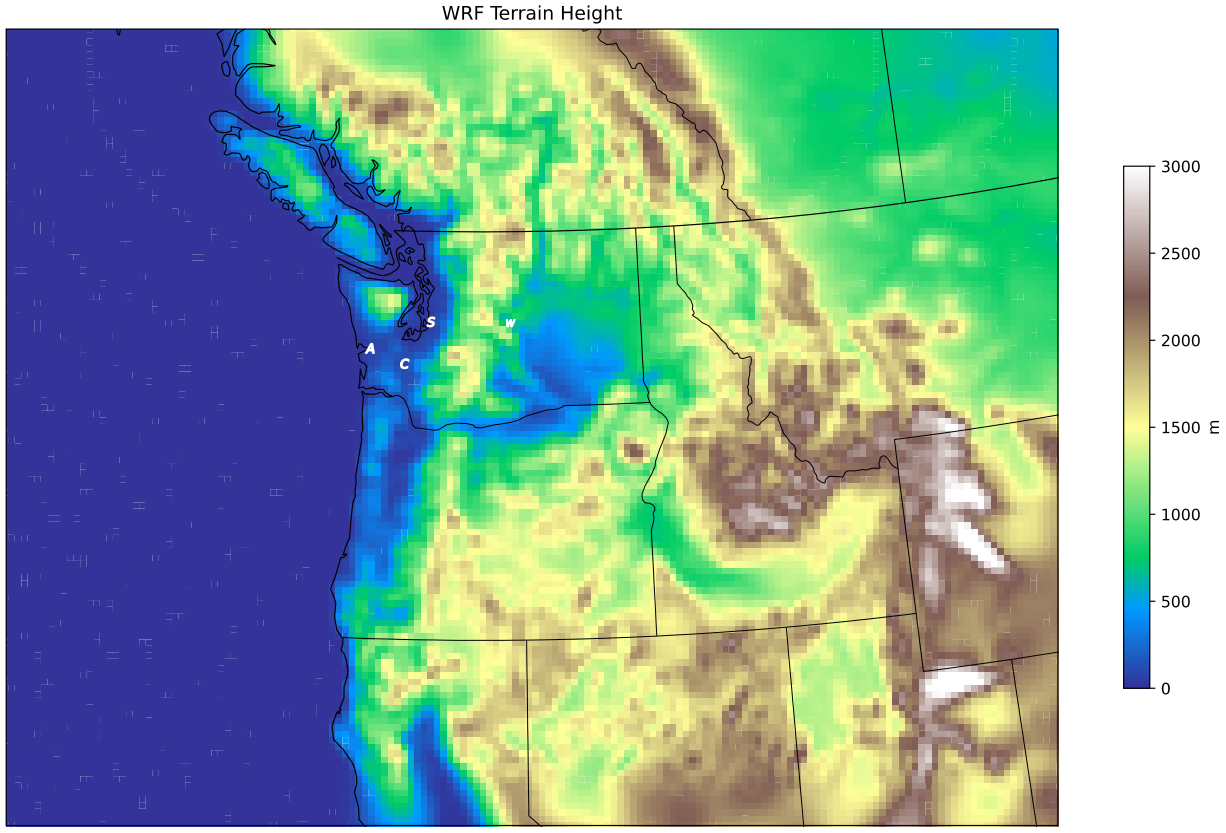

Figure 1. Study region and domain for WRF simulations; shading indicates terrain height on the 12-km WRF grid. Station locations discussed in the text are marked by letters A, C, S, and W.

Full technical details on the regional climate model simulations are given in Mass et al (2022) and the following summary is derived from there with minor modifications. The WRF model configuration used for the climate ensemble has been evaluated n previous studies (Zhang

Accepted for publication in *Journal of Climate*. DOI 10.1175/JCLI-D-22-0313.1

et al. 2009; Duliére et al. 2011), and a similar configuration has been used for numerical weather prediction over the same domain for nearly two decades (Mass et al. 2003). WRF is a non-hydrostatic mesoscale modeling system designed to serve both operational forecasting and atmospheric research (Skamarock et al. 2008) and has been applied extensively for regional climate model (RCM) simulations (e.g., Duffy et al. 2006; Salathé et al. 2014). The simulations presented in this paper applied WRF version 3.8.1 using the following parameterization choices: Thompson microphysics (Thompson and Eidhammer 2014), the Yonsei University (YSU) planetary boundary scheme (Hong et al. 2006), the Grell-Freitas cumulus parameterization (Grell and Freitas 2014), the Rapid Radiative Transfer Model G (RRTMG) for long-wave and short-wave radiation (Iacono et al. 2008), and the Noah-MP land surface (Niu et al. 2011). the 36-km domain is nudged (grid nudging) toward the parent GCM, while the interior 12-km domain is not nudged, but forced on its lateral boundaries by the surrounding coarser (36-km) mesh. Gridded analysis nudging was applied to wind, temperature, and moisture fields above the planetary boundary layer and only wind near the surface. To enhance the model's ability to simulate mesoscale features on the outer domain, nudging coefficients were set to 1/3 the default values for temperature and wind (10^{-4}) and near zero for moisture (10^{-6}). The same WRF model physics options and configuration were used for all members of the high-resolution WRF ensemble.

III. Observed trends from station records

We begin this analysis with the observed daily maximum temperatures at several stations from the Global Historical Climatology Network - Daily Version 3 dataset (Menne et al. 2012); see Table 1 for station information. Station locations are marked in Fig. 1 using the first letter of the station name. Data were obtained from the NOAA Climate Data Online Portal (https://www.ncdc.noaa.gov/cdo-web/). Data were analyzed for the warm-season months May through September. These months were selected since, historically, daily maximum temperatures have exceeded 90°F only during these months. The analysis is done on absolute temperatures, not anomalies relative to the seasonal cycle, since our intention is to focus on the very hottest days of the year, which are associated with a similar dynamical pattern of easterly winds and subsidence warming irrespective of the calendar month.

For each decade, the temperature threshold at several percentiles was found from the 1,530 individual days. We present results for the percentiles 50 (median), 85, 95, 99, and the absolute maximum. The notation *TmaxPct* indicates the daily maximum temperature at the

Accepted for publication in *Journal of Climate*. DOI 10.1175/JCLI-D-22-0313.1

percentile *Pct*; *Tmax50* is the median value and *Tmax99* is the 99th percentile; for notational consistency, *Tmax100* indicates the decadal absolute maximum. The observed daily maximum temperature is greater than or equal to *Tmax99* on 1% of summer days, roughly once in every 100 days, or 15 days per decade. Assuming the probability distribution is stationary within a decade, the percentiles computed over the decade would approximate the theoretical distribution for any single year. However, the decadal period is more likely to sample rare extreme hot days, yielding higher values at the uppermost percentiles than would be found in most years. Decadal absolute maximum (*Tmax100*), in particular, will always be higher than the average of yearly absolute maxima during a decade.

Station	Name	Lat	Lon	Elev (m)
USW00024233	SEATAC	47.4	-122.3	112.8
USC00459074	WENATCHEE	47.4	-120.3	190.8
USC00451276	CENTRALIA	46.7	-123.0	56.4
USC00450008	ABERDEEN	47.0	-123.8	3.0

Table 1. Stations analyzed.

Figure 2 shows the threshold values for each decade and percentile observed at the Sea-Tac airport station, south of Seattle, WA. A linear fit is found for each threshold value, with the lines in Fig. 2 showing the warming trend across the probability distribution. To allow easier comparison of the trends, Fig 2 (right) shows the anomaly temperatures computed relative to the linear fit for the decade 1950-1959. This figure shows differences in the trends at each threshold, with the high extremes showing slightly lower trends than the mean temperature. The linear fit statistics are shown in Table 2. From the low correlation and high p-values of the linear fit, the trends in *Tmax99* and *Tmax100* are not statistically significant. Trends at lower thresholds are weakly statistically significant, and not distinguishable from each other within the error range. As in most other locations, historic trends in daily *Tmin*, which are not discussed here, show statistically significant positive trends at all percentiles. The lack of significance in the upper thresholds is a consequence of the greater degree of random variability in the low sample sizes associated with rare events, which obscures any potential underlying trend. For example, a severe heat event occurred in 2009, matching temperatures observed for the June 2020 event at some stations, yet no severe events occurred in the 2010s. Had the 2009 event occurred a year later, the statistical results would be quite different. Based on these results, it is not possible to reject the hypothesis that recent temperature trends are uniform across percentiles. Alternatively,

Accepted for publication in *Journal of Climate*. DOI 10.1175/JCLI-D-22-0313.1

any effects causing a different warming trend during extreme hot days compared to median days is small compared to natural variability.

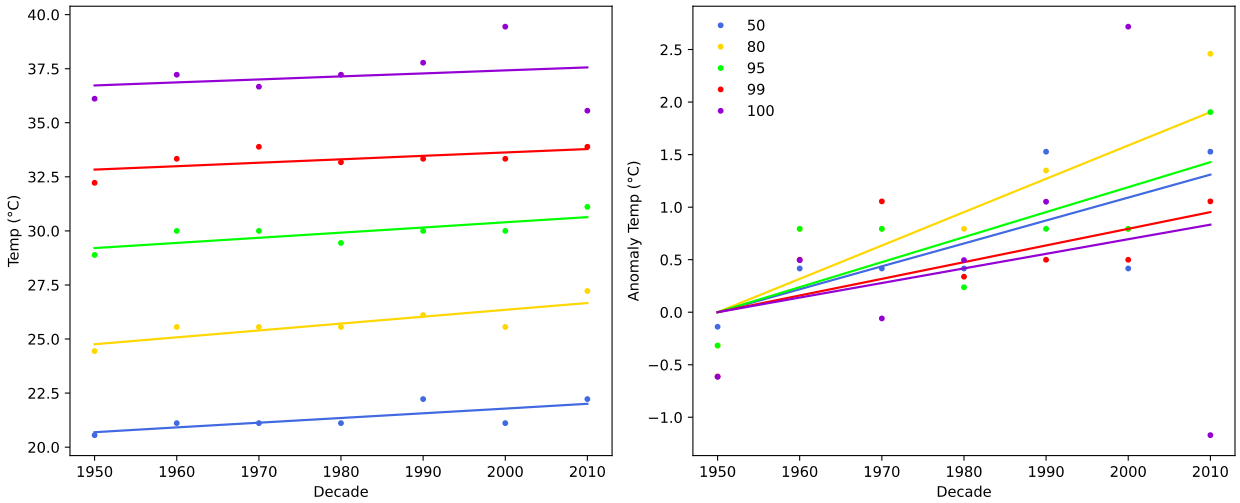

Figure 2. Temperature percentile thresholds for summer-time daily values observed at the Sea-Tac airport station. Values are for the decade starting at the year indicated. The panel on the right shows the anomaly relative to the linear fit valure for the 1950s.

This analysis was repeated for three additional stations: Centralia, WA, which is south of Sea-Tac and lacks the marine influence of Puget Sound; Wenatchee, WA, east of the Cascade Range in the Columbia Plateau; and Aberdeen, WA, on the Pacific coast. Aside from somewhat lower statistical significance of trends at Centralia, the overall warming trends for inland stations are similar and do not show consistent differences by percentile. There is no statistically significant warming in daily maximum temperature observed at Aberdeen over this period due to the moderating influence of the northeastern coastal Pacific, which has not warmed substantially during this period (see, for example, Desbruyères et al. (2017) or NOAA National Centers for Environmental Information (2020)).

Accepted for publication in *Journal of Climate*. DOI 10.1175/JCLI-D-22-0313.1

	Percentile	Slope (°C/decade)	Correlation	P_value
SEATAC	50	0.22	0.75	0.05
	80	0.32	0.83	0.02
	95	0.24	0.76	0.05
	99	0.16	0.61	0.14
	100	0.14	0.24	0.61
WENATCHEE	50	0.20	0.81	0.03
	80	0.22	0.61	0.15
	95	0.22	0.61	0.15
	99	0.27	0.58	0.17
	100	0.22	0.47	0.29
ABERDEEN	50	-0.14	-0.69	0.09
	80	-0.20	-0.81	0.03
	95	0.02	0.20	0.66
	99	0.00	0.01	0.99
	100	-0.08	-0.11	0.82
CENTRALIA	50	-0.06	-0.31	0.50
	80	0.10	0.43	0.34
	95	0.04	0.29	0.53
	99	0.01	0.04	0.94
	100	0.18	0.27	0.56

Table 2. Tmax Regression Statistics for station observations 1950-2019.

IV. Simulated trends from WRF Ensemble

We now turn to a similar analysis of the trends in temperature percentiles simulated in the WRF ensemble for the recent past and projected for the future. Figure 3 shows *Tmax50* (top) and *Tmax99* (bottom) values for each ensemble member and each decade for the Sea-Tac station; colors indicate ensemble members. The black dots and error bars show the ensemble mean and standard deviation for each decade. Relative to the station observations, the WRF ensemble mean has a 4°C warm bias, likely a combination of biases originating the forcing GCMs combined with a warm bias in the WRF simulation (see discussion in Mass et al. 2022). Due to their coarse grids, both the GCM and WRF land masks reduce the influence of Puget Sound, and the elevation of the grid cells are lower than the physical station elevation (even the 12-km WRF grid elevation is too low, 54 m versus 130 m). Both effects would tend to make the WRF temperature higher than observed. Furthermore, there is considerable spread in bias across the ensemble due to differences in the underlying global models, with a standard deviation in the mean of ±1.5°C. At both percentiles, temperatures increase slowly for the first few decades, with a substantially steeper slope following the 2020s. With the exception of the FGOALS-G2 model,

Accepted for publication in *Journal of Climate*. DOI 10.1175/JCLI-D-22-0313.1

all ensemble members show a similar trend, and the ensemble spread does not increase substantially over time, as indicated by the error bars.

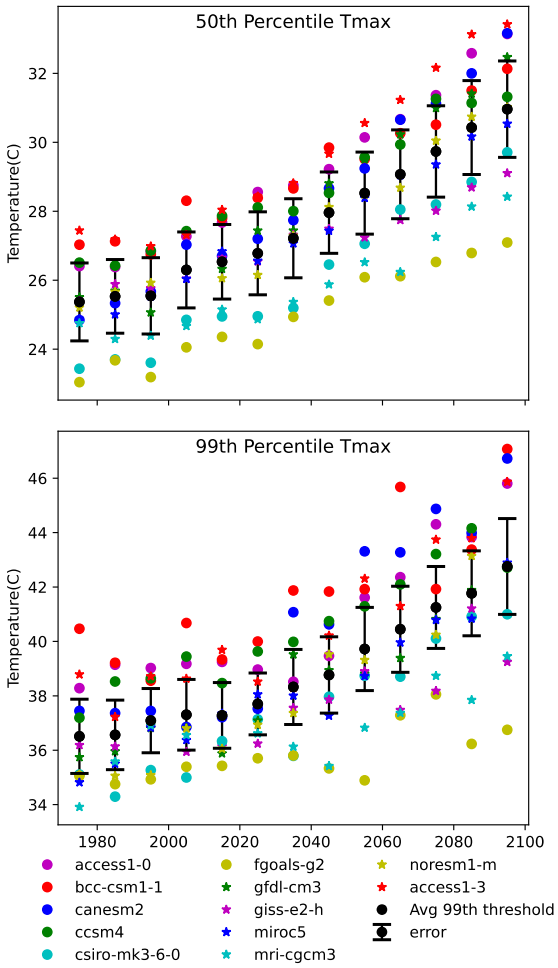

Figure 3. Tmax50 (top) and Tmax99 (bottom) values for each ensemble member and each decade simulated at the Sea-Tac station; colors indicate ensemble members. The black dots and error bars show the ensemble mean and standard deviation for each decade.

Temperature thresholds are computed for 10-year periods, and are subject to considerable sampling noise and internal variability within any single ensemble member, as can be seen in Fig 3. Internal variability remains even computing the percentiles over 30-year periods. In Fig 4, the decadal values of *Tmax99* are compared with values computed from a rolling 30-year interval for two ensemble members, CCSM4 and GISS-E2-H. The 30-year window shows a clear reduction in statistical noise while maintaining cyclic decadal variability around the overall trend, particularly evident in the GISS-E2-H simulation. A single ensemble member can produce substantial variations in the trend of extreme high daily temperatures over time, with prolonged periods of apparent amplified warming or of negligible warming. Since unforced internal

Accepted for publication in *Journal of Climate*. DOI 10.1175/JCLI-D-22-0313.1

variability is independent in each global model, the ensemble mean (Fig 3, black dots) effectively eliminates effects of interannual variability, giving a nearly monotonic increase in *Tmax* thresholds following the external greenhouse gas forcing. The actual trajectory of the future climate, however, will likely contain the much higher variability of individual ensemble members. Given the changing probability distribution of temperatures over time, the 10-year sample used here is a compromise between a short enough period to isolate the warming trend and a long enough period for adequate sampling. Using an ensemble, however, allows for the shorter interval, since in the ensemble mean, a 10-year period includes 120 simulated years.

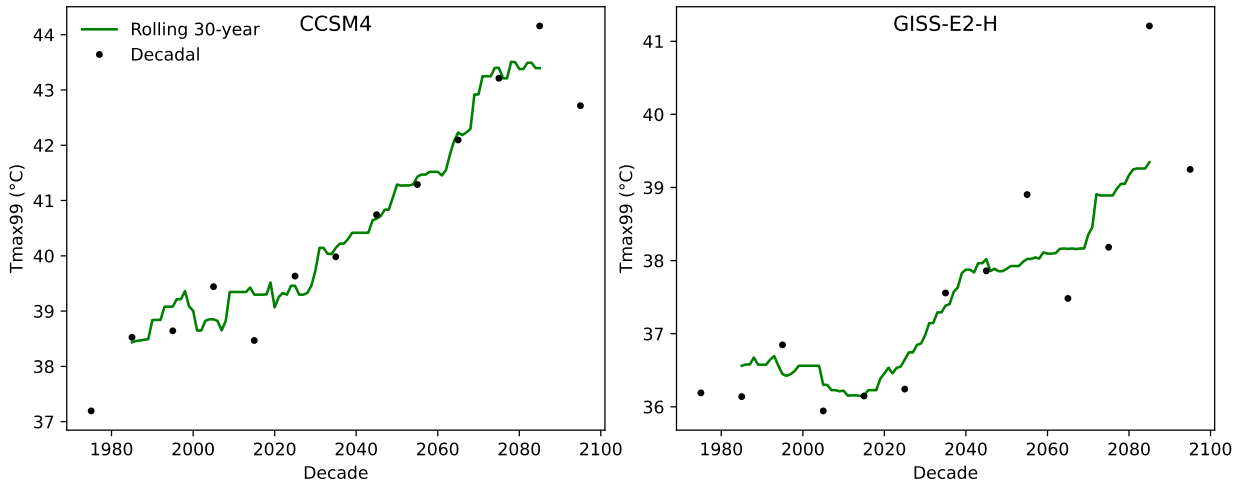

Figure 4. Tmax99 at Sea-Tac simulated in two ensemble members showing the signal of decadal variability. Black dots show decadal means; green lines a running 30-year mean.

Given the upward curvature in the temperature thresholds, we separate the record into two periods 1970-2010 and 2020s-2090s. Based on the residuals, a linear fit is a statistically justified representation of the temporal behavior in each period, and will be used here to characterize the rates of increase. For the period 1970 to 2019, the positive slope in the simulated ensemble-mean *Tmax* percentiles at Sea-Tac (Table 3) is similar to the observed trends for 1950-2019, but with more uniformly positive trends at all percentiles. Since the model ensemble includes 12 samples for each decade, statistical noise and internal variability are substantially reduced relative to the observations, improving the statistical significance of the computed trends. The correlation and p-values indicate moderate to high confidence in the positive trends at all thresholds. However, as with the observations, there is very little difference in the trends for different percentiles, with no indication that the higher percentiles exhibit a larger warming trend than the median. Results for other stations (not shown) are qualitatively similar. The

Accepted for publication in *Journal of Climate*. DOI 10.1175/JCLI-D-22-0313.1

simulated results bolster the case that the lack of clear trends for *Tmax*99 and *Tmax*100 in the observations (Table 2) is the result of natural variability masking an underlying warming tendency across the probability distribution.

Percentile	Slope (°C/decade)	Correlation	P_value
50	0.310	0.936	0.019
80	0.313	0.939	0.018
95	0.240	0.936	0.019
99	0.228	0.934	0.020
100	0.269	0.974	0.005

Table 3. Tmax Regression Statistics for WRF ensemble 1970-2019 at Sea-Tac.

In contrast to the historical period, for the future period (2020-2099), all percentiles show strongly significant positive trends at all stations, as shown graphically for Sea-Tac in Fig 5 and numerically for all stations in Table 4. In all cases, decadal *Tmax* thresholds are highly correlated with time and the linear fit is statistically significant with high confidence. The trend in *Tmax*50 is about double the trend during the 1970-2019 period. Higher percentiles show progressively greater trends than lower percentiles. Furthermore, based on error analysis using a t-test against the standard deviation in the slopes from individual ensemble members, we may reject the hypothesis that the slopes in ensemble-mean *Tmax*50 and *Tmax*99 are equal. For individual ensemble members, however, only 7 out of 12 show a statistically significant difference in the trends at the 50th and 99th percentiles. In the 7 decades from the 2020s to the 2090s, the median temperature (*Tmax*50) at Sea-Tac increases by 4.3°C, while *Tmax*99 increases by 5.1°C and *Tmax*100 by 5.3°C in the ensemble mean.

The results for the Sea-Tac station differ from surrounding locations, illustrating how the specific characteristics of heat wave dynamics and warming trends vary with small distances across the region. In particular, proximity to the ocean has a substantial influence: At Wenatchee, Washington, 150 km to the east and across the Cascade Range on the arid Columbia Plateau, the warming trends are distinctly greater than for Seattle at all percentiles. At Aberdeen, Washington, 125 km to the west-southwest and on the Pacific coast, the warming trends are distinctly lower than for Sea-Tac at all percentiles.

Accepted for publication in *Journal of Climate*. DOI 10.1175/JCLI-D-22-0313.1

	Percentile	Slope (°C/decade)	Correlation	P_value	Difference to 50%
SEATAC	50	0.61	1.00	0.00	0.00
	80	0.64	1.00	0.00	0.03
	95	0.67	1.00	0.00	0.06
	99	0.72	1.00	0.00	0.11
	100	0.76	1.00	0.00	0.15
WENATCHEE	50	0.72	1.00	0.00	0.00
	80	0.78	1.00	0.00	0.06
	95	0.81	1.00	0.00	0.09
	99	0.84	1.00	0.00	0.13
	100	0.84	1.00	0.00	0.12
ABERDEEN	50	0.51	1.00	0.00	0.00
	80	0.51	1.00	0.00	0.00
	95	0.51	0.99	0.00	0.01
	99	0.57	0.98	0.00	0.07
	100	0.67	0.97	0.00	0.17
CENTRALIA	50	0.57	1.00	0.00	0.00
	80	0.63	1.00	0.00	0.06
	95	0.70	1.00	0.00	0.13
	99	0.80	0.99	0.00	0.23
	100	0.83	0.99	0.00	0.26

Table 4. Tmax Regression Statistics for WRF ensemble 2020-2099.

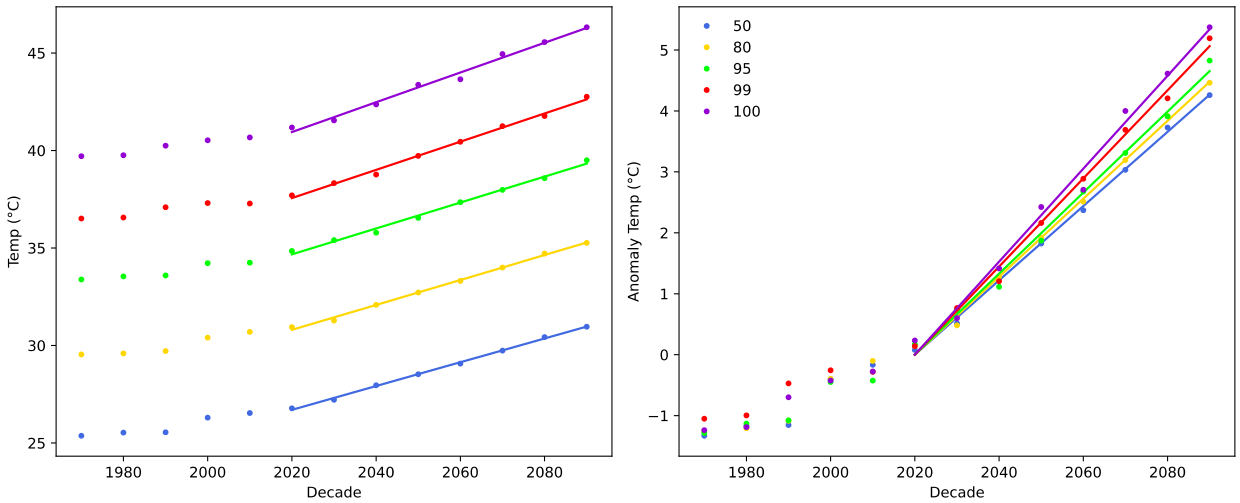

Figure 5. Temperature percentile thresholds for summer-time daily values simulated in the WRF ensemble mean for the Sea-Tac airport station location. Values are for the decade starting at the year indicated. The panel on the right shows the anomaly relative to the linear fit value for the 2020s.

The way trends diverge across temperature percentiles is very different for each of the four stations as well; note the final column in Table 4 indicating how trends for higher temperature thresholds diverge from the median warming. However, the amount of divergence in

Accepted for publication in *Journal of Climate*. DOI 10.1175/JCLI-D-22-0313.1

median and extreme temperatures is not related either to the median temperature or the rate of median warming. Compared to Sea-Tac, trends at Wenatchee are larger at all percentiles, with a similar progression to higher trends at higher percentiles. The high rate of warming at Wenatchee is typical of continental regions and may also reflect land-surface feedbacks that amplify extremes in arid climates (e.g., Seneviratne et al. 2010; Fischer and Schär 2009; Kharin et al. 2018). At Aberdeen on the Pacific coast, lower trends are simulated at all percentiles compared to Sea-Tac on Puget Sound, with little progression to higher warming for higher percentiles except for the absolute hottest days, which show an amplified warming rate. Temperatures at Aberdeen are substantially moderated across the probability distribution by the cool North Pacific waters, which warm slowly with climate change, but this effect may not hold for the absolute warmest days with strong offshore winds. Finally, the warming rate at Centralia, west of the Cascades but away from major water bodies, is similar to Sea-Tac for lower percentiles. However, this station shows substantially greater amplification in the trend for the hottest days, approaching warming rate simulated for Wenatchee. Of the four stations, Centralia shows by far the greatest divergence in temperature trends across percentiles.

To illustrate this complex geographical behavior, Fig 6 shows the difference in the trends of decadal ensemble-mean *Tmax*50 and *Tmax*99 across the full WRF domain. The locations of the four stations discussed above are marked with the initial letter. For much of the interior of the domain, away from complex topography and large water bodies (southern Idaho, Nevada, and Utah), the hot days warm at a similar rate to the median days. However, much of the region exhibits a substantially higher warming rate for hot days than for the median, most obviously in the region around the Cascade Range and Puget Sound. The pattern follows the terrain, with amplification seen on both slopes of the Cascade Range, but particularly on the western slopes. The highest elevations show a reverse effect, with extremes increasing more slowly than the median, likely due to the impact of snow cover on the energy budget. The high-resolution grid nicely resolves the influence of Puget Sound, and the model simulates a moderation in the warming trend for the hottest days over the Puget Sound Basin compared to the surrounding land area.

Accepted for publication in *Journal of Climate*. DOI 10.1175/JCLI-D-22-0313.1

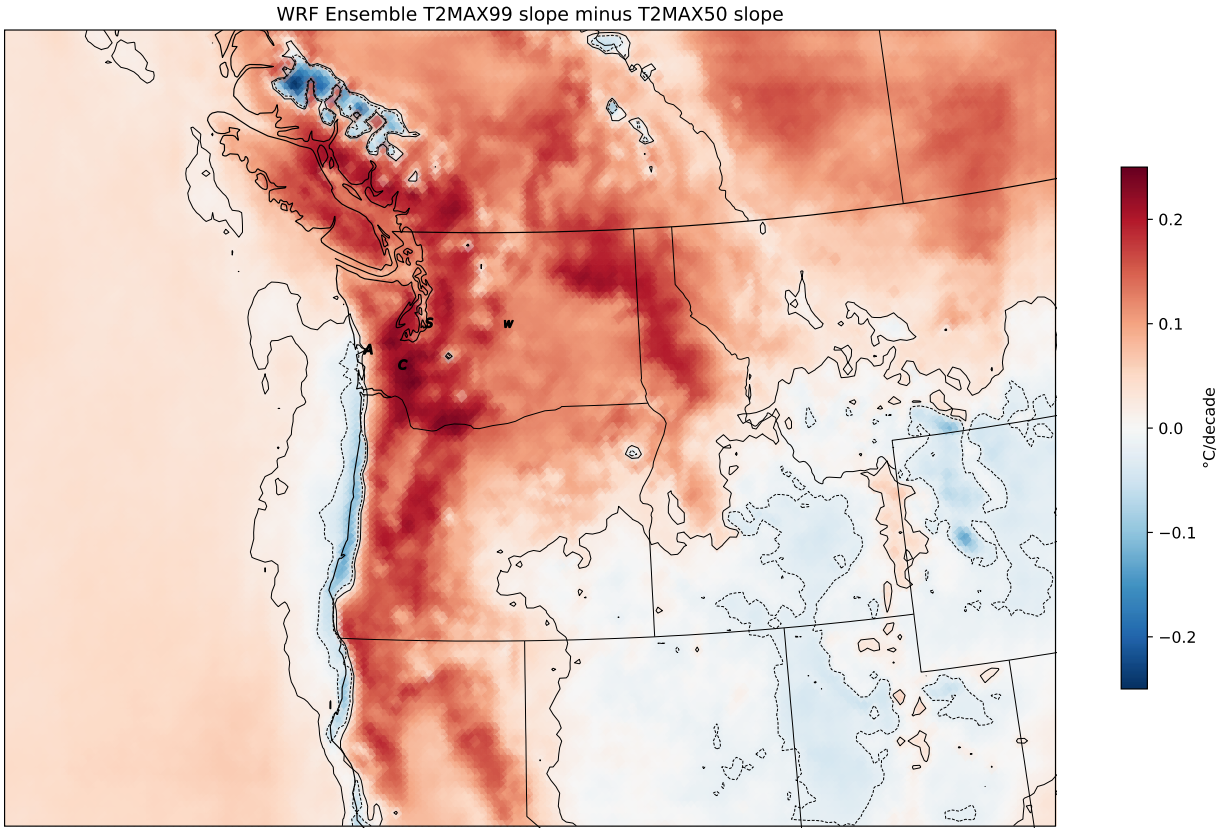

Figure 6. WRF Ensemble mean Tmax99 slope minus Tmax50 Slope for the period 2020-2099. Solid (dashed) contours indicate statistically significant positive (negative) differences.

The terrain barriers show a clear influence on the divergence in warming rates. To illustrate this effect, Fig 7 shows results along two East-West transects. The left panels in Fig. 7 follow a line through Sea-Tac and Wenatchee (marked *S* and *W* in Fig. 6); right panels follow a parallel transect passing through Centralia (marked *C* in Fig. 6). The transects start just off the coast in the west and end at the west slope of the Rocky Mountains in the east. In both transects, we see that the trends in *Tmax*50 and *Tmax*99 are relatively uniform east of the Cascade Range, with the *Tmax*99 slope about 0.1 °C/decade larger. The warming rates for both percentiles decrease and converge over the ocean. For *Tmax*50, the slope drops immediately west of the Cascade crest, converging to the maritime trend. The trend in *Tmax*99, however, remains high across the crest, only dropping at the coast itself.

Accepted for publication in *Journal of Climate*. DOI 10.1175/JCLI-D-22-0313.1

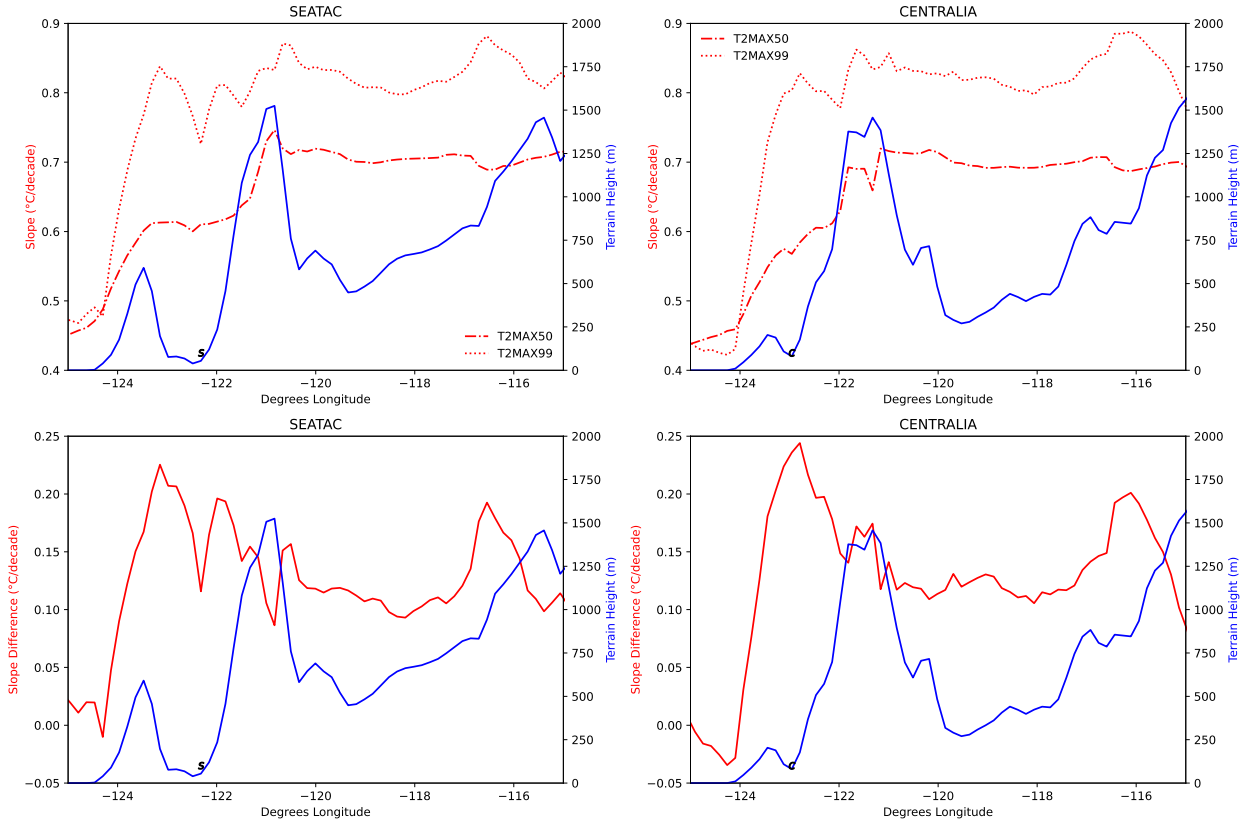

Figure 7. East-west cross sections from Fig 6. Left panels show crossections passing through Sea-Tac; right panels through Centralia .

For the Sea-Tac transect, there is a distinct dip in the slope of *Tmax*99 at Puget Sound (−122.5° longitude), which results in a much smaller difference with the slope of *Tmax*50 compared to surrounding points. Likewise, the effect of the coastal Olympic Mountains at −123.5° longitude appear to limit the influence of the North Pacific on the *Tmax*50 warming rate, which remains uniform between the two barriers. In contrast, in the Centralia transect, the effects of Puget Sound and the Olympics are minimal, and the slope in *Tmax*99 remains high from the Columbia Plateau to the coast while the slope in *Tmax*50 drops quickly from the Cascade Crest, yielding a considerable amplification in the warming of hot days compared to at Sea-Tac. Note the similar amplification on the west slopes of the Rocky Mountains, which suggest this effect is not simply due to easterly winds minimizing a prevailing maritime influence, but also related to adiabatic warming across the terrain.

V. Discussion

The geographical pattern shown above is a clear signature of the documented synoptic and mesoscale conditions during heat waves in the region (Brewer et al. 2013; Bumbaco et al.

Accepted for publication in *Journal of Climate*. DOI 10.1175/JCLI-D-22-0313.1

2013; Chien et al. 1997; Mass et al. 1986). Heat waves in the region are typically associated with the West Coast thermal trough (WCTT) synoptic pattern (see Brewer et al. 2013). These events begin with an upper-level ridge that produces large-scale subsidence and clear skies, warming the surface and lower troposphere. As surface pressure increases in the interior, winds become offshore, producing down slope flow on the west slopes of the major terrain barriers, advecting potential temperature downward and displacing the typical cool maritime air.

A result of the WCTT dynamics is that the daily temperature probability distribution is positively skewed at stations between the coast and the Cascade crest, but not skewed over the ocean nor in the continental interior (Brewer and Mass 2016; Catalano et al. 2021). The temperature distribution is skewed in the same region we show future divergence in the mean and 95% percentile. Given this, the results presented here imply the probability distribution becomes increasingly skewed for land areas west of the Cascades with a warming climate. The simplest explanation is that the skewness relates to the source of airmasses under different circulation patterns. With typical westerly flow, the region west of the Cascades is kept cool by maritime air from the northern Pacific, and we can see in Fig. 7 that the warming rate west of the Cascades during median days is relatively low, following the warming rate over the ocean. During hot WCTT events, air flows into the region from the hotter interior with additional warming due to adiabatic descent, and the warming rate for 99th percentile days west of the Cascades follows the higher warming rate of the continental interior. Thus, the substantially higher median warming rate in the interior compared to the ocean could on its own cause the skewness in daily temperature to increase in a warmer climate.

We discuss two additional mechanisms that could affect the increased skewness simulated for the future by the WRF model: 1) a change in the dynamics during heat events, and 2) regional changes in precipitation.

Modeling results from global climate models (Brewer and Mass 2016) and the WRF ensemble used in this study (Mass et al. 2022) indicate a general weakening of easterly winds. Any weakening of easterly wind during heat events could decrease the temperature skewness, counter to what we find here. Brewer and Mass (2016) show that surface winds at the Cascade Crest are a clear indicator of warming conditions west of the Cascades in the following day, and the simulated winds for a point on the Cascade Crest are used as for Figure 12 in Mass et al (2022) to show a decreasing trend in the simulated number of days per year with easterly winds

Accepted for publication in *Journal of Climate*. DOI 10.1175/JCLI-D-22-0313.1

exceeding 3.4 m/s. Likewise, Catalano et al. (2021) find anomalous mid-tropospheric ridging one to two days prior to warm extremes in the Pacific Northwest, which result in frequent trajectories crossing the Cascades. To examine whether a change in easterly winds affects our results, we show the average 10-m zonal wind speed at the Cascade Crest by decade in Figure 8. The mean for all summer days is shown in blue; the mean for the day preceding any day when the temperature at Sea-Tac exceeds the decadal 99th percentile is shown in red. Dots indicate individual ensemble members and lines the ensemble median. From Figure 8 it is clear that while westerly (positive) zonal winds prevail during summer, heat events at Sea-Tac are strongly associated with easterly (negative) zonal winds at the Cascade Crest. While there is a modest decrease in summertime-mean winds, the magnitude of easterly winds associated with heat events at Sea-Tac shows no trend over the projection. A similar null result is found for changes in the frequency and intensity of ridging events in the CMIP6 global models (Loikith et al. 2022). Thus, it appears that heat-wave dynamics do not change significanly during the period when temperature skewness increases.

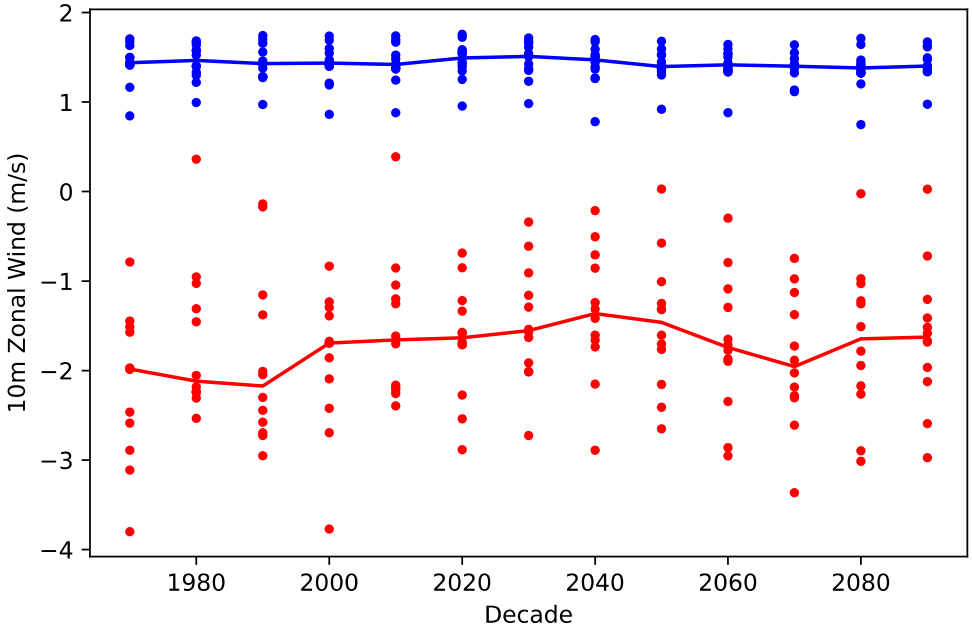

Figure 8. Average 10-m winds at the Cascade Crest for all summer days (Blue) and during days when temperature exceeds the 99th percentile at Sea-Tac (red). Dots are individual ensemble members and lines are the ensemble median.

An additional mechanism could be related to changes in precipitation. As shown in Mass et al. (2022, Figure 7), summertime precipitation is projected to decrease west of the Cascades and increase slightly in many regions east of the Cascades. The fractional change in summertime

Accepted for publication in *Journal of Climate*. DOI 10.1175/JCLI-D-22-0313.1

precipitation from 1970-1999 to 2070-2099 along the same transects as in Fig 7 is shown in Fig. 9. Precipitation generally decreases by 20 to 30% where the simulation shows the largest divergence in the trends of *Tmax*50 and *Tmax*99, with small changes where the divergence is smaller. The patterns are not fully aligned, however, and it is not clear that changes in precipitation or associated cloud cover would have a greater impact on the temperature of hot days than on median days. However, it is plausible that with lower precipitation and decreased soil moisture, the moderating effect of evapotranspiration would decrease especially on the hottest days with an amplifying soil moisture temperature feedback (Seneviratne et al. 2010).

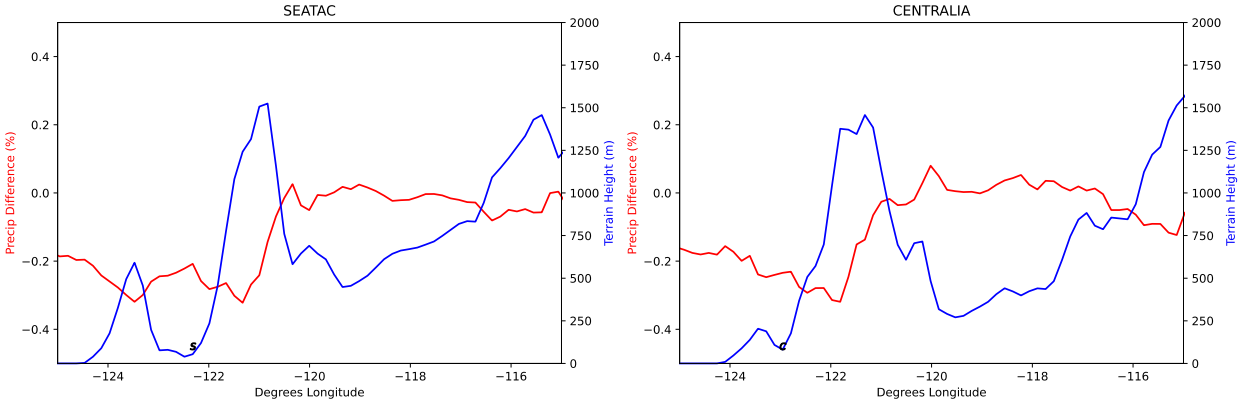

Figure 9. Fractional change in simulated precipitation from 1970-1999 to 2070-2099 along the east-west cross sections as for Fig 7. Left panels show crossections passing through Sea-Tac; right panels through Centralia.

VI. Conclusions

The modeling results presented above indicate quite clearly that at some locations, the temperature on the warmest days may warm at a higher rate than on median days in the future. This behavior, however, is far from universal even within the study domain and is closely related to the effects of topography and land-water contrasts. Several mesoscale effects could be responsible for the simulated geographical patterns. First, west of the Cascade Range, the warming rate during median days appears to be moderated by the cool North Pacific and onshore flow while the warming rate during the hottest days appears to be amplified by easterly flow across the Cascade crest. Secondly, the interior plateau warms at a substantially higher rate than the coastal zone, especially during the hottest days. In addition, it is possible that changes in precipitation or cloud cover may be contributing to the warming trends. Taken together, these results indicate that the future warming rate during heat events in western Washington could be controlled by non-local mesoscale feedbacks and circulation patterns. Understanding future heat

Accepted for publication in *Journal of Climate*. DOI 10.1175/JCLI-D-22-0313.1

events in the populated regions west of the Cascades requires understanding the feedbacks during extreme heat events both locally and across the Cascades, which establish the warming trend of these events.

The differences in the trends shown here are statistically significant, but in a practical sense, are small enough that they could be masked by natural variability in the actual evolution of the atmosphere. Furthermore, these trends are only evident due to the strong climate response simulated for the end of the century with the RCP8.5 scenario. Arguably, the simulated increased rate of warming during 99th percentile days, of less than 0.2°C per decade may not create significantly greater impacts than would be found based on the trend in the median daily maximum temperature. However, the evidence that the warming rate during extreme events in one location is linked to a distant set of feedbacks in the land-atmosphere system is significant. Additionally, rare events like the heat wave in June 2021 have the greatest impacts. These events are outside the range of recent experience and do not allow for natural adaptation and acclimatation to changing climate. To the extent that extreme heat events are connected to climate processes far away increases the plausibility that future heat events will not conform to recent experience, shattering records.

Acknowledgments

Undergraduate students, A. Beggs, C McJunkin, and S. Sandhu participated in this work as part of the UW Bothell Physics REU Funded by National Science Foundation Award #2050928. E. Salathé was supported by the National Science Foundation under Grant AGS-2040626 and by the UW Bothell SRCP Seed Grant Program. WRF simulations were supported by an Amazon Catalyst grant, which provided both personnel support and computer resources through Amazon Web Services.

Data Availability Statement

The regional climate model simulations made for this study are archived on a RAID disk array in the UW Atmospheric Sciences department. They can be made available through either anonymous FTP or by providing a hard disk for data sets to be transferred to.

Accepted for publication in *Journal of Climate*. DOI 10.1175/JCLI-D-22-0313.1

VII. References

Brewer, M. C., and C. F. Mass, 2016: Projected changes in heat extremes and associated synoptic- and mesoscale conditions over the Northwest United States. J Clim, 29, 6383–6400, https://doi.org/10.1175/JCLI-D-15-0641.1.

Brewer, M. C., C. F. Mass, and B. E. Potter, 2012: The West Coast Thermal Trough: Climatology and Synoptic Evolution. *Mon Weather Rev*, **140**, 3820–3843, https://doi.org/10.1175/MWR-D-12-00078.1.

Brewer, M. C., C. F. Mass, and B. E. Potter, 2013: The West Coast Thermal Trough: Mesoscale Evolution and Sensitivity to Terrain and Surface Fluxes. *Mon Weather Rev*, **141**, 2869–2896, https://doi.org/10.1175/mwr-d-12-00305.1.

Bumbaco, K. A., K. D. Dello, and N. A. Bond, 2013: History of Pacific Northwest Heat Waves: Synoptic pattern and trends. *J Appl Meteorol Climatol*, **52**, 1618–1631, https://doi.org/10.1175/JAMC-D-12-094.1.

Catalano, A. J., P. C. Loikith, and J. D. Neelin, 2021: Diagnosing Non- Gaussian Temperature Distribution Tails Using Back- Trajectory Analysis. *Journal of Geophysical Research: Atmospheres*, **126**, https://doi.org/10.1029/2020JD033726.

Chien, F.-C., C. F. Mass, and Y.-H. Kuo, 1997: Interaction of a Warm-Season Frontal System with the Coastal Mountains of the Western United States. Part I: Prefrontal Onshore Push, Coastal Ridging, and Alongshore Southerlies. *Mon Weather Rev*, **125**, 1705–1729, https://doi.org/10.1175/1520-0493(1997)125<1705:IOAWSF>2.0.CO;2.

Desbruyères, D., E. L. McDonagh, B. A. King, and V. Thierry, 2017: Global and Full-Depth Ocean Temperature Trends during the Early Twenty-First Century from Argo and Repeat Hydrography. *J Clim*, **30**, 1985–1997, https://doi.org/10.1175/JCLI-D-16-0396.1.

Donat, M. G., and L. v. Alexander, 2012: The shifting probability distribution of global daytime and night-time temperatures. *Geophys Res Lett*, **39**, https://doi.org/10.1029/2012GL052459.

Duffy, P. B., and Coauthors, 2006: Simulations of Present and Future Climates in the Western United States with Four Nested Regional Climate Models. *J Clim*, **19**, 873–895, https://doi.org/10.1175/JCLI3669.1.

Duliére, V. R., Y. Zhang, and E. P. Salathé, 2011: Extreme precipitation and temperature over the U.S. Pacific Northwest: A comparison between observations, reanalysis data, and regional models. *J Clim*, **24**, 1950–1964, https://doi.org/10.1175/2010JCLI3224.1.

Accepted for publication in *Journal of Climate*. DOI 10.1175/JCLI-D-22-0313.1.

Fischer, E. M., and C. Schär, 2009: Future changes in daily summer temperature variability: Driving processes and role for temperature extremes. *Clim Dyn*, **33**, 917–935, https://doi.org/10.1007/s00382-008-0473-8.

Fischer, E. M., S. Sippel, and R. Knutti, 2021: Increasing probability of record-shattering climate extremes. *Nat Clim Chang*, **11**, 689–695, https://doi.org/10.1038/S41558-021-01092-9.

Folland, C. K., and Coauthors, 2001: Observed Climate Variability and Change. Climate Change 2001: The Scientific Basis. Contribution of Working Group I to the Third Assessment Report of the Intergovernmental Panel on Climate Change, J.T., Houghton, Y. Ding, D.J. Griggs, M. Noguer, P.J. van der Linden, X. Dai, and C.A.J. K. Maskell, Eds., Cambridge University Press, p. 881pp.

Grell, G. A., and S. R. Freitas, 2014: A scale and aerosol aware stochastic convective parameterization for weather and air quality modeling. *Atmos Chem Phys*, **14**, 5233–5250, https://doi.org/10.5194/acp-14-5233-2014.

Hong, S.-Y., Y. Noh, and J. Dudhia, 2006: A New Vertical Diffusion Package with an Explicit Treatment of Entrainment Processes. *Mon Weather Rev*, **134**, 2318–2341, https://doi.org/10.1175/mwr3199.1.

Iacono, M. J., J. S. Delamere, E. J. Mlawer, M. W. Shephard, S. A. Clough, and W. D. Collins, 2008: Radiative forcing by long-lived greenhouse gases: Calculations with the AER radiative transfer models. *Journal of Geophysical Research Atmospheres*, **113**, https://doi.org/10.1029/2008JD009944.

Kharin, V. v., G. M. Flato, X. Zhang, N. P. Gillett, F. Zwiers, and K. J. Anderson, 2018: Risks from Climate Extremes Change Differently from 1.5°C to 2.0°C Depending on Rarity. *Earths Future*, **6**, 704–715, https://doi.org/10.1002/2018EF000813.

Klein, T., J. M. Torres-Ruiz, and J. J. Albers, 2022: Conifer desiccation in the 2021 NW heatwave confirms the role of hydraulic damage. *Tree Physiol*, https://doi.org/10.1093/treephys/tpac007.

Loikith, P. C., D. Singh, and G. P. Taylor, 2022: Projected Changes in Atmospheric Ridges over the Pacific–North American Region Using CMIP6 Models. *J Clim*, **35**, 5151–5171, https://doi.org/10.1175/JCLI-D-21-0794.1.

Accepted for publication in *Journal of Climate*. DOI 10.1175/JCLI-D-22-0313.1

Mass, C. F., M. D. Albright, and D. J. Brees, 1986: The Onshore Surge of Marine Air into the Pacific Northwest: A Coastal Region of Complex Terrain. *Mon Weather Rev*, **114**, 2602–2627, https://doi.org/10.1175/1520-0493(1986)114<2602:TOSOMA>2.0.CO;2.

——, and Coauthors, 2003: Regional environmental prediction over the pacific nothwest. *Bull Am Meteorol Soc*, **84**, 1353-1366+1328, https://doi.org/10.1175/BAMS-84-10-1353.

——, E. P. Salathé, R. Steed, and J. Baars, 2022: The Mesoscale Response to Global Warming over the Pacific Northwest Evaluated Using a Regional Climate Model Ensemble. *J Clim*, **35**, 2035–2053, https://doi.org/10.1175/JCLI-D-21-0061.1.

Menne, M. J. , and Coauthors, 2012: Global Historical Climatology Network - Daily (GHCN-Daily), Version 3. *NOAA National Climatic Data Center.* , https://doi.org/10.7289/V5D21VHZ.

Niu, G. Y., and Coauthors, 2011: The community Noah land surface model with multiparameterization options (Noah-MP): 1. Model description and evaluation with local-scale measurements. *Journal of Geophysical Research Atmospheres*, **116**, https://doi.org/10.1029/2010JD015139.

NOAA National Centers for Environmental Information, 2020: State of the Climate: Global Climate Report for 2019. https://www.ncdc.noaa.gov/sotc/global/201913/supplemental/page-3 (Accessed March 14, 2022).

Overland, J. E., 2021: Causes of the Record-Breaking Pacific Northwest Heatwave, Late June 2021. *Atmosphere (Basel)*, **12**, 1434, https://doi.org/10.3390/atmos12111434.

Rhines, A., and P. Huybers, 2013: Frequent summer temperature extremes reflect changes in the mean not the variance. *Proc Natl Acad Sci U S A*, **110**, https://doi.org/10.1073/pnas.1218748110.

Salathé, E. P., A. F. Hamlet, C. F. Mass, S.-Y. Lee, M. Stumbaugh, and R. Steed, 2014: Estimates of Twenty-First-Century Flood Risk in the Pacific Northwest Based on Regional Climate Model Simulations. *J Hydrometeorol*, **15**, 1881–1899, https://doi.org/10.1175/JHM-D-13-0137.1.

Seneviratne, S. I., T. Corti, E. L. Davin, M. Hirschi, E. B. Jaeger, I. Lehner, B. Orlowsky, and A. J. Teuling, 2010: Investigating soil moisture-climate interactions in a changing climate: A review. *Earth Sci Rev*, **99**, 125–161, https://doi.org/10.1016/j.earscirev.2010.02.004.

Accepted for publication in *Journal of Climate*. DOI 10.1175/JCLI-D-22-0313.1

——, M. G. Donat, B. Mueller, and L. v. Alexander, 2014: No pause in the increase of hot temperature extremes. *Nat Clim Chang*, **4**, 161–163, https://doi.org/10.1038/nclimate2145.

Skamarock, W. C., and Coauthors, 2008: A description of the Advanced Research WRF Version 3, NCAR Technical Note TN-475+STR. 113 pp.

Taylor, K. E., R. J. Stouffer, and G. A. Meehl, 2012: An overview of CMIP5 and the experiment design. *Bull Am Meteorol Soc*, **93**, 485–498, https://doi.org/10.1175/BAMS-D-11-00094.1.

Thompson, G., and T. Eidhammer, 2014: A Study of Aerosol Impacts on Clouds and Precipitation Development in a Large Winter Cyclone. *J Atmos Sci*, **71**, 3636–3658, https://doi.org/10.1175/jas-d-13-0305.1.

Zhang, Y., V. Duliére, P. W. Mote, and E. P. Salathé, 2009: Evaluation of WRF and HadRM mesoscale climate simulations over the U.S. Pacific Northwest. *J Clim*, **22**, 5511–5526, https://doi.org/10.1175/2009JCLI2875.1.

Accepted for publication in *Journal of Climate*. DOI 10.1175/JCLI-D-22-0313.1